Physical Chemistry Chemical Physics
CREATED USING THE RSC LaTeX PCCP ARTICLE TEMPLATE – SEE www.rsc.org/electronicfiles FOR DETAILS
View Article Online
DOI: 10.1039/C7CP03575F
ARTICLE TYPE
www.rsc.org/xxxxxx | XXXXXXXX

First principles study of $p-$type defects in $LaCrO_3$

Samira Dabaghmanesh,*[a,b,c] Nasrin Sarmadian,[a] Erik C. Neyts[b] and Bart Partoens[a]

Recently, Sr-doped $LaCrO_3$ has been experimentally introduced as a new *p-type* transparent conducting oxide. It is demonstrated that substituting Sr for La results in inducing p-type conductivity in $LaCrO_3$. Performing first principles calculations we study the electronic structure and formation energy of various point defects in $LaCrO_3$. Our results for the formation energies show that in addition to Sr, two more divalent defects, Ca and Ba, substituting for La in $LaCrO_3$ behave as shallow acceptors in line with previous experimental reports. We further demonstrate that under oxygen-poor growth conditions, these shallow acceptors will be compensated by intrinsic donor-like defects (oxygen vacancy and Cr on an oxygen site), but in the oxygen-rich growth regime the shallow acceptors have the lowest formation energies between all considered defects and will lead to *p*-type conductivity.

1 Introduction

Transparent conducting oxides (TCOs) have a wide range of applications, for example in transparent electrodes for touch screens, light emitting diodes (LEDs), and as top layer in solar cells.[1–5] However, many potential applications of TCOs are hindered by the lack of *p*-type TCOs, as needed, for example, in the fabrication of transparent p-n junctions. The development of transparent *p*-type electrodes is also required for a more efficient hole collection in photovoltaic cells.[1]

Since more than two decades many different *p*-type TCOs have been developed, including Cu^+-based delafossites $CuMO_2$ (M=B, Al, Cr, Ga, Sc, In, and Y), layered oxychalcogenides LaCuOCh (Ch= S, Se, Te), and d^6 spinel oxides AB_2O_4 (A=tetrahedrally coordinated Mg, Zn, Cd; B= octahedrally coordinated Co, Rh, Ir), for more details see Ref. 6 and references therein. However, developing efficient *p*-type TCOs is challenging due to the intrinsic electronic structure of oxides which leads to a large hole effective mass and consequently a low conductivity in most of these *p*-type TCOs. This large hole effective mass of oxides originates from the localized $2p$ states of oxygen that form the top of the valence band.

Recently, perovskite Sr-doped $LaCrO_3$ (LCO) has been reported as a *p*-type TCO.[7] LCO is an insulating material that has its strongest optical absorption at ≈ 4.6 eV, which makes it optically transparent[8]. It has been experimentally shown that substituting Sr^{2+} for La^{3+} in LCO can significantly dope holes into the top of the valence band and results in the *p*-type conductivity. The authors of Ref. 7 have demonstrated that the conductivity of $La_{1-x}Sr_xCrO_3$ increased from 1.2 S cm^{-1} to 54 S cm^{-1} by increasing the concentration of Sr from $x = 0.04$ to $x = 0.5$[7] which is among the best values reported for *p*-type TCOs[6]. An insulator-to-metal transition has also been observed in $La_{1-x}Sr_xCrO_3$ at $x \geq 0.65$.[9]

The good chemical and thermal stability of the perovskite structure allow the easy dopability of LCO and the easy combination with other perovskite *n*-type TCOs offering a promising candidate for p-n junction applications with coherent p-n interfaces. For instance the perovskite $SrTiO_3$ which can be easily doped *n*-type[10–12] is shown to form a coherent interface with *p*-type doped LCO.[13] Doped LCO can also be a potential candidate for the contact material in the perovskite solar cells which are recently identified as a new class of solar cell materials.[14]

To support the optical absorption measurements of Sr-doped LCO in Ref. 9 density of states (DOS) calculations of different alloying concentrations of Sr were also performed. However, defect calculations of LCO are still lacking. In this work we study the electronic and structural properties of Sr-doped LCO using first principles calculations, and investigate the shallow or deep character of Sr as a potential acceptor in LCO. We also investigate the intrinsic donor-like defects, namely oxygen vacancy and Cr on an O site that may act as killer defects in Sr-doped LCO.

Moreover also alkaline-earth doped LCO has been the subject of intensive experimental and theoretical research because of its applications in solid oxide fuel cells.[15–18] It has been reported that the electrical conductivity of LCO can be improved by its doping with Ca and Ba suggesting it as an interesting system for solid oxide fuel cells.[17,18] Therefore, in addition to the Sr dopant we investigate the effect of two more divalent dopants, namely Ca and Ba belonging to the same group as Sr but with different ionic radius, on the conductivity of LCO.

The paper is further organized as follows. In Sec. 2 we discuss the density functional theory used in our calculations. In Sec. 3 we first present our results of bulk LCO and provide details about the considered calculation method for the defect calculations, then the results of the defect calculations are pre-

[a] *Department of Physics, University of Antwerp, Groenenborgerlaan 171, B-2020 Antwerpen, Belgium*
[b] *Research Group PLASMANT, Department of Chemistry, University of Antwerp, Universiteitsplein 1, B-2610 Antwerp, Belgium.*
[c] *SIM vzw, Technologiepark 935, BE-9052 Zwijnaarde, Belgium.*
* E-mail: samira.dabaghmanesh@uantwerpen.be

View Article Online
DOI: 10.1039/C7CP03575F

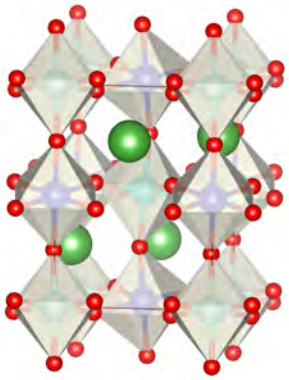

Fig. 1 Unit cell of orthorhombic perovskite $LaCrO_3$ with the G-type antiferromagnetic arrangement of the Cr^{3+} ions. La ions are shown in green and oxygen ions in red spheres. The positions of the Cr ions in spin up and spin down are indicated as light and dark blue spheres, respectively.

sented in Sec. 4. Finally we summarize our conclusions in Sec. 5.

2 Methods

All calculations in the present work are performed within the density functional theory (DFT) approach using the Vienna *Ab-initio* Simulation Package (VASP).[19–21] The plane-wave basis set and the projector augmented-wave method[22] have been used to obtain the structural and electronic properties of pure and doped LCO. A plane wave cut-off energy of 450 eV is used for the plane-wave basis set. To sample the Brilluin zone a $6\times6\times4$ and a $2\times2\times2$ Γ-centered Monkhorst-Pack grids[23] based on convergence tests are used for the primitive unit cell, and the defect supercells, respectively. For the density of states calculations a k-point of $9\times9\times6$ is used. In the geometry optimization a convergence criterion for the forces on the atoms of less than 0.01 eV/Å is considered.

To study the defects in LCO, we constructed a $3\times3\times2$ supercell containing 360 atoms. Although hybrid functionals are known to be very reliable for defect calculations, they would be extremely costly for the required LCO supercell size. Therefore, we first examine the performance of the generalized gradient approximation (GGA) of Perdew-Burke-Ernzerhof (PBE).[24] In order to correct the strong electronic correlation of the Cr 3d states, we also calculate the electronic properties of bulk LCO with the empirical PBE+U approach[25], using different U values for the Cr 3d states, and comparing the results with experimental one and those obtained using the Heyd, Scuseria, Ernzerhof (HSE06) hybrid functional.[26,27] We performed spin polarized calculations for all the considered functionals. As we show, the PBE+U functional with U= 3.3 eV for Cr 3d states describes the bulk electronic structure of LCO properly, and therefore it is used in the following defect calculations.

We calculate the formation energy ($E_f[X^q]$) for a defect X in charge state q as a function of the Fermi energy E_F and the chemical potential μ of La, Cr, O, Sr, Ba, and Ca applying the supercell method[28] using

$$E_f[X^q] = E_{tot}[X^q] - E_{tot}[\text{bulk}] - \sum_i n_i\mu_i + q[E_F + E_v + \Delta V] \quad (1)$$

$E_{tot}[X^q]$ is the total energy of the supercell that contains defect, and $E_{tot}[\text{bulk}]$ is the total energy of the equivalent pure supercell. n_i indicates the number of atoms of type i that have been added to ($n_i>0$) or removed ($n_i<0$) from the supercell when the defect is created, and μ_i is the corresponding chemical potential which represents the energy of the reservoir with which atoms are being exchanged. E_F is the Fermi energy with respect to the valence band maximum (VBM) of the primitive unit cell, E_v. ΔV is the difference in the reference potential of the supercell with and without defect.[28] We calculate ΔV following the procedure introduced in Ref. 29. In order to determine the nature of the thermodynamic transition levels (shallow or deep) of each considered defect we calculate the position of the transition levels, $\varepsilon(q,q')$, between different charge states q and q' using their formation energies. The transition level between charge states q and q' occurs at the Fermi energy at which the formation energies of q and q' are equal.

3 Bulk $LaCrO_3$

Bulk LCO has an orthorhombic perovskite structure (space group Pbnm) with 20 atoms in the unit cell as shown in Fig. 1. It has a G-type anti-ferromagnetic insulating ground state below its Néel temperature (275 K).[32–34] Each Cr^{3+} ion has three occupied t_{2g}^3 states in high-spin configuration which is hybridized with $2p$ states of neighboring oxygen atoms, while the three other t_{2g}^0 states and all e_g^0 states are empty. The authors of Ref. 8 show that the lowest energy transition in LCO originates from the Mott-Hubbard type transition $t_{2g}^3 \longrightarrow e_g^0$ at ≈ 2.8 eV. As this transition is dipole forbidden, it was overlooked in earlier experimental reports of the band gap.[32,35] The strongest optical absorption appears at ≈ 4.6 eV which is due to the O $2p \longrightarrow$ Cr 3d charge-transfer excitation.[8]

The electronic structure of bulk LCO has been investigated using DFT+U[36] and HSE06[37] functionals reporting different values of the band gap. The optimal values of the Hubbard-U parameter in the DFT+U study and the α parameter (i.e. the fraction of exact Hartree-Fock exchange included in the exchange correlation functional) in the HSE06 calculations were determined in order to produce the experimental optical band gap, which was reported as 3.4 eV, in the early experimental works.[32,35] As in more recent experimental measure-

View Article Online
DOI: 10.1039/C7CP03575F

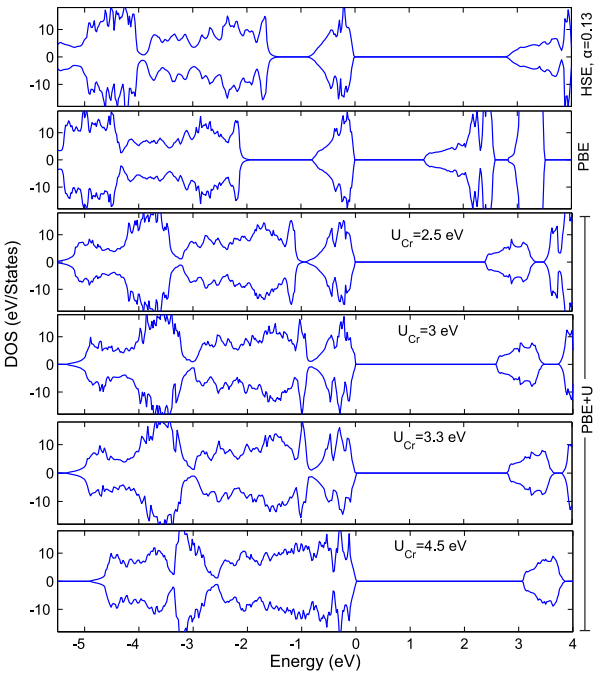

Fig. 2 Calculated total DOS of $LaCrO_3$ using HSE06, PBE, and PBE+U using different U values for Cr 3*d* states.

ments[8] the lowest transition has been observed at 2.8 eV, we recalculate the electronic structure of bulk LCO using PBE, PBE+U, and HSE06 calculations. We optimize the values of the Hubbard-U and the α parameters to obtain the band gap of 2.8 eV for LCO. Beside yielding the correct band gap of LCO, the selected functional for the study of a *p*-type TCO should also predict the correct character of the VBM. In order to study the effect of different functionals on these two parameters we calculate the projected density of states (PDOS) of LCO using HSE06 and PBE+U functionals.

The calculated DOS are shown in Fig. 2, and the corresponding lattice parameters, magnetic moments and band gaps are listed in Table 1. We find the optimum value for $\alpha = 0.13$ which gives band gap of 2.8 eV in agreement with the experimental value. We note that this value of α is smaller than the value ($\alpha = 0.15$) reported in Ref. 37 which is adjusted to produce the gap of 3.4 eV. The PBE calculation underestimates the band gap of 2.8 eV by 1.4 eV. Within the PBE+U method the best agreement with HSE06 and the experimental band gap is obtained using U= 3.3 eV which is lower than the value of U= 4.5 eV reported in another theoretical study.[36] Table 1 shows that the calculated lattice parameters and magnetic moments using PBE+U (U= 3.3 eV) are in good agreement with the corresponding HSE06 and experimental values.

The calculated PDOS obtained with the PBE+U and the HSE06 functionals are shown in Fig. 3. Based on the optical absorption spectrum of Ref. 8, we know that the VBM of LCO is dominated by occupied Cr 3*d* (t_{2g}^3) states with a minor contribution of O 2*p* states, while empty Cr 3*d* (e_g^0) states form the conduction band minimum (CBM). Both calculated PDOS show the contribution of Cr 3*d* and O 2*p* in the VBM and CBM, in agreement with experiment. The DOS projected on t_{2g}^3 and e_g states of one Cr are shown in the insets of Figs. 3(a) and 3(b). As we can see each Cr 3*d* orbital splits into an occupied $t_{2g\uparrow}^3$ states (at the VBM) and unoccupied $e_{g\uparrow}$, $t_{2g\downarrow}$, and $e_{g\downarrow}$ states (at the CBM) which agrees with the absorption spectrum and the calculated PDOS reported in Ref. 8 using the B3LYP functional. We notice that a second gap in the valence band is present in the HSE06 DOS, which closes in the corresponding PBE+U result.

We calculate the band gap and character of the VBM, as two

Table 1 Optimized lattice parameters a, b, c (in Å), magnetic moment μ (in $\mu_B/atom$), and direct band gap E_g (in eV) of bulk LCO, for different DFT functionals (PBE, PBE+U, HSE06) and the corresponding experimental values. The U parameters are in units of eV.

Method	a	b	c	μ	E_g
PBE	5.52	5.50	7.78	2.61	1.28
PBE+U (U= 2.5)	5.56	5.54	7.84	2.79	2.41
PBE+U (U= 3)	5.56	5.56	7.84	2.82	2.65
PBE+U (U= 3.3)	5.57	5.54	7.84	2.87	2.81
PBE+U (U= 4.5)	5.59	5.56	7.87	3.01	3.12
HSE06 ($\alpha = 0.13$)	5.51	5.50	7.77	2.78	2.82
Experiment	5.51	5.47	7.75*	2.85**	2.8***

*Ref. 30, **Ref. 31, ***Ref. 8

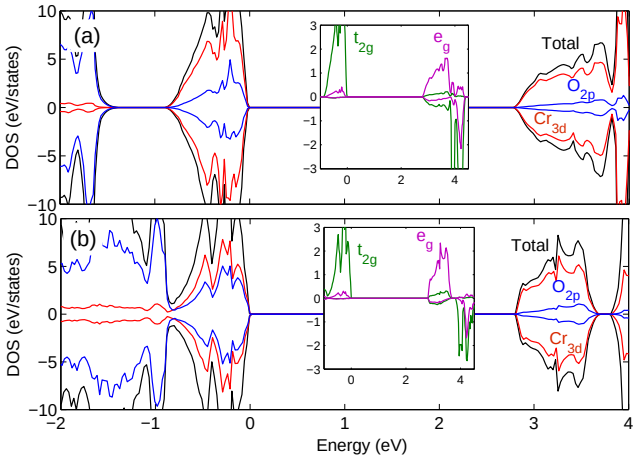

Fig. 3 PDOS of $LaCrO_3$ calculated using (a) HSE06, and (b) PBE+U. The total DOS, Cr 3*d*, O 2*p*, Cr t_{2g}, and Cr e_g states are shown in black, red, blue, green, and pink, respectively.

View Article Online
DOI: 10.1039/C7CP03575F

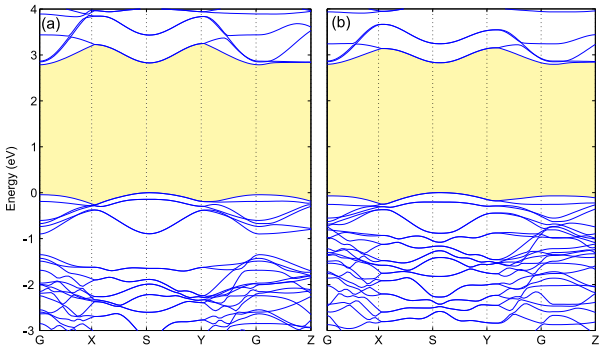

Fig. 4 Electronic band structure of orthorhombic perovskite $LaCrO_3$ calculated using (a) HSE06 and (b) PBE+U (U= 3.3 eV). The VBM is aligned to 0.

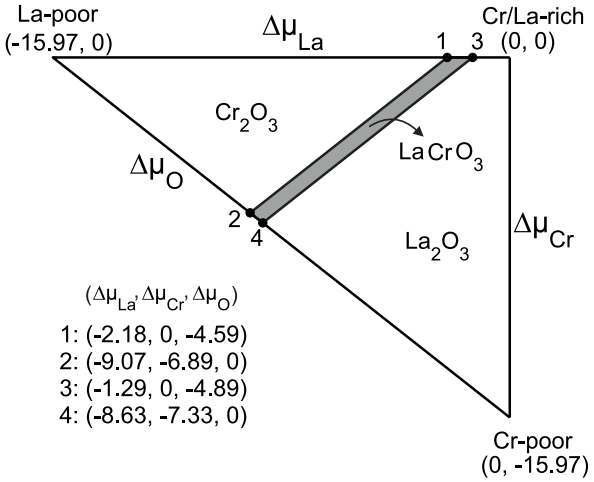

Fig. 5 Illustration of accessible chemical potential range for $LaCrO_3$.

most important characteristics for description of hole properties in a TCO, that agree with the corresponding experimental values. Furthermore, the experimental study of Sr-doped LCO[9], at high doping concentrations, is also supported by the DOS calculations obtained using the DFT+U method. The implemented U= 3 eV in Ref. 9 correctly reproduces the DOS of the Sr-doped LCO in good agreement with the experimental results. The selected U value is close to what we obtained (U= 3.3 eV) by comparing the band gap and VBM character of bulk LCO with the experimental results. Therefore, we apply PBE+U using U= 3.3 eV for the further study of defects in LCO.

The band structures of LCO calculated using HSE06 and PBE+U using the selected U= 3.3 eV are compared in Fig. 4. In Ref. 37, based on a HSE06 calculation with $\alpha = 0.15$, it is stated that LCO has a direct band gap at Γ. We find a fundamental indirect band gap with the VBM at S and the CBM at Γ in both HSE06 and PBE+U calculated band structures. However, we should note that the VBM values at S and Γ are very close. The system possesses an indirect band gap of $E_g^{\mathrm{PBE+U}} = 2.79$ eV, and $E_g^{\mathrm{HSE06}} = 2.78$ eV while its direct band gap is at S and has a magnitude of $E_g^{\mathrm{PBE+U}} = 2.81$ eV, and $E_g^{\mathrm{HSE06}} = 2.82$ eV. We also calculate the hole effective mass at the VBM using the PBE+U method. We find 2.26 m_e and 2.71 m_e along the (010) and (100) directions, respectively. Although these hole effective mass values are still large compared to their counterparts in well-known *n*-type TCOs (e.g. the electron effective masses of In_2O_3, ZnO and SnO_2 are around 0.2-0.35 m_e [3,38,39]), they are much lower than those of the well-known *p*-type TCOs (e.g. $CuCrO_2$, $CuScO_2$ and $SrCu_2O_2$ have hole effective masses around 4-7 m_e [40,41]).

In order to make sure that the selected PBE+U (U= 3.3 eV) can correctly predict the magnetic ground state of bulk LCO, we also compared three more magnetic configurations for the Cr atoms in addition to the AFM-G state, namely ferromagnetic (FM), and two antiferromagnetic AFM-A and AFM-C orderings. We found that the selected value for U indicates the AFM-G as the most stable magnetic configuration in agreement with experimental results.[32–34]

4 Defects in $LaCrO_3$

Thermodynamic stability of $LaCrO_3$

According to Eq. (1) the defect formation energy depends on the chemical potential μ_i of each atomic species. Considering different chemical potentials, we can study the effect of varying experimental growth conditions. For each atomic species the chemical potential is defined by $\mu_i = \mu_i^{(0)} + \Delta\mu_i$, where $\mu_i^{(0)}$ is the chemical potential of element i in its stable phase (i.e. bulk of La, Cr, Sr, Ba, and Ca and diatomic molecule of O). The chemical potentials are related to the enthalpy of formation of the oxide host through $\Delta H_f[LaCrO_3] = \Delta\mu_{\mathrm{La}} + \Delta\mu_{\mathrm{Cr}} + 3\Delta\mu_{\mathrm{O}} = -15.97$ eV. In order to avoid the precipitation into the constituent bulk of La, Cr, and O_2 gas we require $\Delta\mu_{\mathrm{La}} \leq 0$, $\Delta\mu_{\mathrm{Cr}} \leq 0$, $\Delta\mu_{\mathrm{O}} \leq 0$. From these conditions one can calculate the three vertices of a triangle area, known as stability triangle, which correspond to Cr/O-rich ($\Delta\mu_{\mathrm{La}} = -15.97$ eV, $\Delta\mu_{\mathrm{Cr}} = 0$, $\Delta\mu_{\mathrm{O}} = 0$), La/O-rich ($\Delta\mu_{\mathrm{La}} = 0$, $\Delta\mu_{\mathrm{Cr}} = -15.97$ eV, $\Delta\mu_{\mathrm{O}} = 0$), and La/Cr-rich ($\Delta\mu_{\mathrm{La}} = 0$, $\Delta\mu_{\mathrm{Cr}} = 0$, $\Delta\mu_{\mathrm{O}} = -15.97$ eV) conditions. The resulting accessible range of the chemical potentials are illustrated in Fig. 5 in the $(\Delta\mu_{\mathrm{La}}, \Delta\mu_{\mathrm{Cr}})$ plane.

The chemical potentials are further constrained by the segregation of $LaCrO_3$ into competing binary phases which are La_2O_3 and Cr_2O_3. Therefore, the conditions $2\Delta\mu_{\mathrm{La}} + 3\Delta\mu_{\mathrm{O}} \leq \Delta H_f[La_2O_3]$ and $2\Delta\mu_{\mathrm{Cr}} + 3\Delta\mu_{\mathrm{O}} \leq \Delta H_f[Cr_2O_3]$ should be ful-

View Article Online
DOI: 10.1039/C7CP03575F

Table 2 Calculated chemical potentials of Sr, Ca, and Ba at the chemical potential limits imposed by formation of binary oxides SrO, CaO, and BaO under different growth conditions as indicated in Fig. 5. All energies are in eV.

	$\Delta\mu_{Sr}$	$\Delta\mu_{Ca}$	$\Delta\mu_{Ba}$
La-poor	-5.494	-5.952	-4.975
Cr-poor	-5.494	-5.952	-4.975
vertex1	-0.901	-1.359	-0.382
vertex2	-5.494	-5.952	-4.975
vertex3	-0.603	-1.062	-0.085
vertex4	-5.494	-5.952	-4.975

filled. Taking into account the constraints imposed by the competing binary phases, the stable range of $\Delta\mu_{La}$, $\Delta\mu_{Cr}$, and $\Delta\mu_{O}$ has been obtained from the calculated formation energies of $\Delta H_f[La_2O_3] = -17.267$ eV and $\Delta H_f[Cr_2O_3] = -13.78$ eV under O-rich, Cr-rich, and La-rich conditions. These constraints result in the grey area in Fig. 5 which is the range of chemical potentials in which LCO is thermodynamically stable against its segregation into the competing binary phases, La_2O_3 and Cr_2O_3. Note that we also considered two more binary oxides of Cr (i.e. CrO and CrO_2) in the calculation of the stability triangle in Fig. 5 but only the smallest area obtained from all considered binaries are shown, corresponding to La_2O_3 and Cr_2O_3. The exact chemical potential values of $\Delta\mu_{La}$, $\Delta\mu_{Cr}$, and $\Delta\mu_{O}$ at the vertices 1,2,3 and 4 are listed in Fig. 5. These values are used in Eq. (1) to calculate the formation energies plotted in Fig. 6.

In the case of Sr, Ca, and Ba doping another constraint is also imposed to avoid the formation of SrO, CaO and BaO: $\Delta\mu_{Sr}+\Delta\mu_{O} \leq \Delta H_f[SrO]$, $\Delta\mu_{Ca}+\Delta\mu_{O} \leq \Delta H_f[CaO]$, and $2\Delta\mu_{Ba}+\Delta\mu_{O} \leq \Delta H_f[CaO]$. The chemical potentials of the extrinsic defects Sr, Ca, and Ba are also determined under various conditions as indicated in Fig. 5 using calculated formation energies of $\Delta H_f[SrO] = -5.494$ eV, $\Delta H_f[CaO] = -5.952$ eV, and $\Delta H_f[BaO] = -4.975$ eV. The calculated values of $\Delta\mu_{Sr}, \Delta\mu_{Ba}$, and $\Delta\mu_{Ca}$ are also listed in Table 2.

Defect formation energies and transition levels

We consider the defect formation energy of three extrinsic point defects Sr, Ba, and Ca substituting La (Sr_{La}, Ba_{La}, and Ca_{La}) which are expected to act as acceptor defects in LCO. Using the Goldschmidt rules for perovskites[42,43] we obtain the tolerance factors 0.94, 1.02, and 0.89, respectively, for the substitution of the three alkaline-earth metals Sr, Ba, and Ca with La in LCO. These values are close to unity indicating that the perovskite structure of LCO remains stable under the doping with the considered alkaline-earth metals.[17,18]

To investigate whether *p*-type conductivity in LCO would not be hindered by the presence of donor defects, we also consider the O vacancy (V_O) and the Cr substitution onto an O site (Cr_O) as potential compensating donor defects. The formation of the neutral oxygen vacancy in $La_{0.6}Sr_{0.4}CrO_3$ has been studied in Ref. 44. The defect formation energies corresponding to O-poor (vertex 1 in Fig. 5) and O-rich (vertex 2 in Fig. 5) conditions are given as a function of the Fermi energy in Figs. 6(a) and 6(b), respectively.

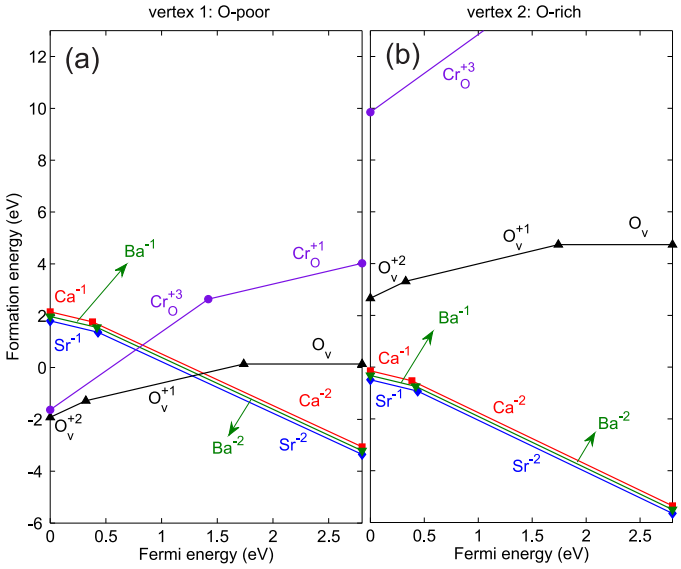

Fig. 6 Defect formation energies of Ca_{La}, Sr_{La}, Ba_{La}, V_O, and Cr_O as a function of Fermi energy under (a) O-poor, and (b) O-rich conditions.

All three considered dopants Sr_{La}, Ca_{La}, and Ba_{La} behave as shallow acceptors. Their charge state is -1 at the Fermi energies close to the VBM that leads to a *p*-type conductivity. Note that their formation energies are also surprisingly similar. This can be understood from the similar ionic radii of these three alkali metals (namely 1.12 Å, 1.26 Å, and 1.47 Å for Ca, Sr, and Ba, respectively[45]). As shown in Fig. 6(a), both V_O as well as Cr_O defects act as killer defects, pinning the Fermi energy deep in the band gap in O-poor conditions. However, under O-rich growth conditions, none of these intrinsic defects can act as killer defect, as shown in Fig. 6(b), and consequently Ca_{La}, Sr_{La}, and Ba_{La} are uncompensated for all values of the Fermi energy. All these three defects have very low formation energies, so that they can be easily formed under O-rich conditions and therefore contribute in the *p*-type conductivity in LCO. This is in line with the experimental findings mentioned above[7,9,17] which report an induced *p*-type conductivity by substituting of trivalent La by divalent Sr, Ca, and Ba.

The shallow acceptor character of the Sr_{La}, Ca_{La}, and Ba_{La} can be understood as follows. Figure 7 shows the PDOS of the neutral relaxed supercell of LCO that contains a Sr impurity. One can see a small peak, close to the VBM, indicating

View Article Online
DOI: 10.1039/C7CP03575F

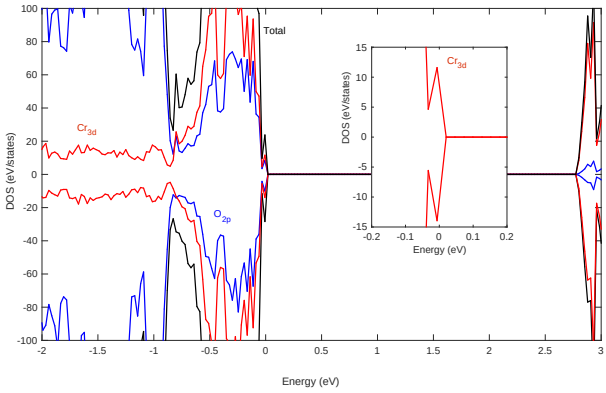

Fig. 7 Calculated total and projected density of states of Sr-doped $LaCrO_3$. The inset shows a enlargement around the VBM.

a localized defect level. The observed peak has Cr character. In the -1 charge state of Sr, the corresponding peak gets filled, and relaxation further lowers the energy which leads to the hybridization of this level with the valence band. Since Sr has one valence electron less than La, it can provide one electron less towards the oxygen ions around it. Some Cr^{3+} ions have turned into Cr^{4+} ions, compensating the missing electron. It is experimentally observed that the transition of Cr^{3+} to Cr^{4+} gradually increased by increasing the concentration of Sr which is consistent with the VBM character of LCO consisting of Cr t_{2g}^3 levels[9,33] (see Fig. 3). Moreover, we find that the magnetic moments ($\pm$2.84, $\mp$2.82) decrease for the four Cr ions surrounding the Sr dopant with respect to the magnetic moments of the Cr atoms in the bulk LCO (Table 1). This is also an indication of the change of these Cr ions from Cr^{3+} to Cr^{4+}. Similarly, the local magnetic moments of the four Cr ions surrounding the Ca ($\pm$2.83, $\mp$2.82) and Ba ($\pm$2.86, $\mp$2.82) are slightly reduced compared to the bulk values (Table 1).

To make sure whether the AFM-G magnetic configuration remains the magnetic ground state in presence of dopants we performed additional calculations for Sr/Ba/Ca-doped LCO. We have examined three more magnetic orderings, i.e., FM, AFM-A, and AFM-C, in addition to the AFM-G magnetic ordering. We considered supercell containing one defect per 72 formula units (360 atoms). The results are summarized in Table 3 (the AFM-G type is taken as the reference energy). We indeed find that introducing dopants in LCO does not alter the ground state magnetic ordering with respect to its bulk.

5 Concluding remarks

Using first principles calculations, we first studied the electronic and structural properties of LCO, then we performed formation energy calculations for different type of point defects in LCO. We examined PBE, PBE+U, and HSE06 methods by comparing the calculated electronic band structures as well as total DOS and PDOS of LCO. We found that PBE+U using U$=$ 3.3 eV for Cr 3*d*-states gives a band gap of 2.79 eV close to the corresponding HSE06 value of 2.8 eV and in very good agreement with the experimental band gap of 2.8 eV. Furthermore, from the calculated PDOS, we observed that both HSE06 and PBE+U methods predict the same Cr t_{2g}^3 VBM character. Therefore, we used the PBE+U method to perform the defect formation calculations. Regarding to the recent experimental work which reports Sr-doped LCO as a *p*-type TCO, we performed defect formation energy calculations for Sr, Ca, and Ba dopants as well as for the intrinsic defects, namely V_O and Cr_O. We demonstrated that Sr, Ca, and Ba defects act as shallow acceptors in LCO. Under O-poor conditions, they are compensated by the intrinsic donors. However, in O-rich conditions, doping with Sr, Ca or Ba are not compensated by potential donor-like defects. Due to their very low formation energies these defects can easily grow and provide holes in LCO to realize a *p*-type TCO.

Table 3 The energy of Sr/Ba/Ca-doped LCO, i.e. one defect in LCO supercell containing 72 formula units, for different magnetic configurations. The energies are in eV and the AFM-G ordering is taken as the reference.

	FM	AFM-A	AFM-C	AFM-G
Sr-doped	2.679	1.749	0.690	0
Ba-doped	2.703	1.778	0.693	0
Ca-doped	2.641	1.727	0.680	0

Acknowledgements. This work was supported by SIM vzw, Technologiepark 935, BE-9052 Zwijnaarde, Belgium, within the InterPoCo project of the H-INT-S horizontal program. The computational resources and services were provided by the Flemish Supercomputer Center and the HPC infrastructure of the University of Antwerp (CalcUA), both funded by the FWO-Vlaanderen and the Flemish Government.

References

1 E. Fortunato, D. Ginley, H. Hosono and D. C. Paine, *MRS Bull.*, 2007, **32**, 242.
2 R. M. P. Barquinha, L. Pereira and E. Fortunato, Transparent Oxide Electronics: From Materials to Devices 1st edn (Chichester: Wiley).
3 T. Minami, *Semicond. Sci. Technol.*, 2005, **20**, 3544.
4 C. G. Granqvist, *Sol. Energy Mater. Sol. Cells*, 2007, **91**, 1529.
5 G. Frank, E. Kauer and H. Kostlin, *Thin Solid Films*, 1981, **77**, 107.

View Article Online
DOI: 10.1039/C7CP03575F

6 K. H. L. Zhang, K. Xi, M. G. Blamire and R. G. Egdell, *J. Phys.: Condens. Matter*, 2016, **28**, 383002.
7 K. H. L. Zhang, Y. Du, A. Papadogianni, O. Bierwagen, S. Sallis, L. F. J. Piper, M. E. Bowden, V. Shutthanandan, P. V. Sushko and S. A. Chambers, *Adv. Mater.*, 2015, **27**, 5191.
8 P. V. Sushko, L. Qiao, M. Bowden, T. Varga, G. J. Exarhos, F. K. Urban, D. Barton and S. A. Chambers, *Phys. Rev. Lett.*, 2013, **110**, 077401.
9 K. H. L. Zhang, Y. Du, P. V. Sushko, M. E. Bowden, V. Shutthanandan, S. Sallis, L. F. J. Piper and S. A. Chambers, *Phys. Rev. B*, 2015, **91**, 155129.
10 W. Luo, W. Duan, S. G. Louie and L. Cohen, *Phys. Rev. B*, 2004, **70**, 214109.
11 T. Higuchi and T. Tsukamoto, *Phys. Rev. B*, 1998, **57**, 6978.
12 L. Triggiani, A. B. Muñoz-García, A. Agostianoab and M. Pavone, Phys. Chem. Chem. Phys., 2016, **18**, 28951.
13 S. A. Chambers, L. Qiao, T. C. Droubay, T. C. Kaspar, B. W. Arey and P. V. Sushko, *Phys. Rev. Lett.*, 2011, **107**, 206802.
14 M. Pazoki, T. J. Jaccobsson, A. Hagfeldt, G. Boschloo and T. Edvinsson, *Phys. Rev. B*, 2016, **93**, 144105.
15 Hui Qi, *Inorg. Chem., Commun.*, 2016, **66**, 33.
16 B. A. Boukamp, *Nat. Mater.*, 2003, **2**, 294.
17 K. P. Ong, P. Wu, L. Liu and P. Jiang, *Appl. Phys. Lett.*, 2007, **90**, 044109.
18 S. P. Jiang, L. Liua, K. P. Ong, P. Wu, J. Li, J. Puc, *J. Power Sources*, 2008, **176**, 82.
19 G. Kresse and J. Hafner, *Phys. Rev. B*, 1994, **49**, 14251.
20 G. Kresse and J. Furthmuller, *Comput. Mater. Sci.*, 1996, **6**, 15.
21 G. Kresse and J. Furthmuller, *Phys. Rev. B*, 1996, **54**, 11169.
22 P. E. Blöchl, *Phys. Rev. B*, 1994, **50**, 17953.
23 H. J. Monkhorst and J. D. Pack, *Phys. Rev. B*, 1976, **13**, 5188.
24 J. Perdew, K. Burke and M. Ernzerhof, *Phys. Rev. Lett.*, 1996, **77**, 3865.
25 S. L. Dudarev, G. A. Botton, S. Y. Savrasov, C. J. Humphreysn and A. P. Sutton, *Phys. Rev. B*, 1998, **57**, 1505.
26 J. Heyd, G. E. Scuseria and M. Ernzerhof, *J. Chem. Phys.*, 2003, **118**, 8207.
27 A. V. Krukau, O. A. Vydrov, A. F. Izmaylov and G. E. Scuseria, *J. Chem. Phys.*, 2006, **125**, 224106.
28 C. G. Van de Walle and J. Neugebauer, *J. Appl. Phys.*, 2004, **95**, 3851.
29 M. N. Amini, R. Saniz, D. Lamoen and B. Partoens, *J. Appl. Phys.*, 2011, **110**, 063521.
30 J. Yang , *Acta Cryst.*, 2008, B**64**, 281.
31 E. F. Bertaut, J. Mareschal, G. De Vries, R. Aleonard, R. Pauthenet, J. P. Rebouillat and V. Zarubicka, *IEEE Trans. Magn.*, 1966, **2**, 453.
32 T. Arima, Y. Tokura and J. B. Torrance, *Phys. Rev. B*, 1993, **48**, 17006.
33 K. Maiti and D. D. Sarma, *Phys. Rev. B*, 1996, **54**, 7816.
34 W. C. Koehler and E. O. Wollan, *J. Phys. Chem. Solids*, 1957, **2**, 100.
35 T. Arima and Y. Tokura, *J. Phys. Soc. Jpn.*, 1995, **64**, 2488.
36 Z. Q. Yang, Z. Huang and L. Ye, X. Xie, *Phys. Rev. B*, 1999, **60**, 15674.
37 J. HE, C. Franchini, *Phys. Rev. B*, 2012, **86**, 235117.
38 P. P. Edwards, A. Porch, M. O. Jones, D. V. Morgan and R. M. Perks, *Dalton Trans.*, 2004, 2995.
39 K. H. L. Zhang, V. K. Lazarov, T. D. Veal, F. E. Oropeza, C. F. McConville, R. G. Egdell and A. Walsh, *J. Phys.: Condens. Matter*, 2011, **23**, 334211.
40 D. O. Scanlon and G. W. Watson, *J. Mater. Chem.*, 2011, **21**, 3655.
41 D. O. Scanlon, K. G. Godinho, B. J. Morgan and G. W. Watson, *J. Chem. Phys.*, 2010, **132**, 024707.
42 V. M. Goldschmidt, Geochemische Verteilungsgesetze der Elemente VIIVIII, Norske Videnskaps Akademi, 1926, Oslo, Skrifter.
43 T. J. Jaccobsson, M. Pazoki, A. Hagfeldt and T. Edvinsson, *J. Phys. Chem. C*, 2015, **119(46)**, 25673.
44 A. M. Deml, V. Stevanović, C. L. Muhich, C. B. Musgrave and R. O'Hayre, *Energy Environ. Sci.*, 2014, **7**, 1996.
45 R. D. Shannon, *Acta Crystallogr. A*, 1976, **32**, 751.